ELSEVIER

International Journal of Heat and Fluid Flow 20 (1999) 149–157

International Journal of HEAT AND FLUID FLOW

Developing convective heat transfer in deep rectangular microchannels

Todd M. Harms, Michael J. Kazmierczak *, Frank M. Gerner

Department of Mechanical, Industrial, and Nuclear Engineering, University of Cincinnati, Cincinnati, OH 45221-0072, USA

Received 13 April 1998; accepted 28 October 1998

Abstract

Experimental results have been obtained for single-phase forced convection in deep rectangular microchannels. Two configurations were tested, a single channel system and a multiple channel system. The two systems are identical except for the lack of extended surfaces in the single channel system. In the case of the multiple channel system the channels are 251 μm wide and the channel walls are 119 μm thick. In both systems the channels are approximately 1000 μm deep and define a projected area of 2.5 cm × 2.5 cm. All tests were performed with deionized water as the working fluid, where the Reynolds number ranged from 173 to 12 900. The experimentally obtained local Nusselt number agrees reasonably well with classical developing channel flow theory. Furthermore, the results show that, in terms of flow and heat transfer characteristics, our microchannel system designed for developing laminar flow outperforms the comparable single channel system designed for turbulent flow.

Keywords: Microchannels; Developing heat transfer; Forced convection; Electronic cooling

Notation

A	area available for convection, Eq. (24), cm^2
b	channel height, μm
c_p	specific heat of water at constant pressure, kJ/kg °C
D_h	hydraulic diameter, $2w_{ch}b/(w_{ch}+b)$, μm
f	fanning friction factor, Eq. (4)
f_{app}	apparent friction factor, Eq. (5)
f_{turb}	turbulent friction factor, Eq. (6)
G	rectangular channel friction factor correction, Eq. (7)
h	local heat transfer coefficient, Eq. (23), W/m^2 °C
K_∞	incremental pressure drop number, Eq. (8)
k_{Si}	thermal conductivity of silicon, W/m °C
k_w	thermal conductivity of water, W/m °C
l_{ch}	channel length, cm
l_h	heater length, cm
mb	fin parameter, Eq. (17)
N	number of channels
Nu	local Nusselt number, Eq. (12)
$Nu_{N=1}$	Nusselt number for $N=1$, Eq. (11)
Nu_{turb}	turbulent Nusselt number, Eq. (13)
Pr	Prandtl number of water
q	heater power, W
Q	volumetric flow rate of water, cm^3/s
R	local system resistance, Eq. (21), °C/W
R_{ch}	channel resistance, Eq. (19), °C/W
R_{sub}	substrate resistance, Eq. (20), °C/W
Re	channel Reynolds number, Eq. (2)
s	thickness of the substrate, μm
T_h	heater temperature, Eq. (22), °C
T_m	mean water temperature, Eq. (15), °C
$T_{m,i}$	inlet water temperature, °C
$T_{m,o}$	outlet water temperature, °C
T_w	temperature at the silicon–water interface, Eq. (25),°C
U_m	mean fluid velocity, $Q/(Nw_{ch}b)$, m/s
w_{cc}	total width of the channel core, cm
w_{ch}	channel width, μm
w_h	heater width, cm
w_w	channel wall width, μm
X^*	dimensionless axial distance for the thermal entrance region, Eq. (10)
x^+	dimensionless axial distance for the hydrodynamic entrance region, Eq. (3)
x, y, z	Cartesian coordinates, cm

Greek

α	channel aspect ratio, Eq. (1)
Δp	total pressure drop, kPa
Δp_{ch}	channel core pressure drop, kPa
ϵ	channel surface roughness, μm
η	fin efficiency, Eq. (18)
μ_m	viscosity of water evaluated at T_m, kg/m s
μ_w	viscosity of water evaluated at T_w, kg/m s
ν	kinematic viscosity of water, m^2/s
ρ	density of water, kg/m^3
τ_{wall}	wall shear stress, kPa

* Corresponding author. E-mail: mike.kazmiercak@uc.edu.

0142-727X/99/$ – see front matter
PII: S0142-727X(98)10055-3

1. Introduction

The emergence of micro-electro-mechanical systems or MEMS has generated significant interest in the area of microscale heat transfer. Etched microchannel heat exchangers, a subfield within MEMS, are of interest because of their extremely high heat flux capability. This ability makes microchannels well-suited for a wide variety of unique cooling applications. Unfortunately, the small hydraulic diameter responsible for the large heat flux also leads to a relatively high pressure drop. As such, careful attention must be given to balance the flow and heat transfer attributes of microchannel systems.

Microchannels are normally produced by either precision machining or chemical etching. In the past, etched microchannels ranged from 150 to 320 μm in depth. Using novel etching techniques (Hölke, 1998), 1000 μm deep microchannels have been fabricated and tested as a part of this study. These are the deepest, etched microchannels reported in the literature for the purpose of heat transfer enhancement. Although microchannels of similar depth have been developed by precision machining techniques (for example, Sasaki and Kishimoto, 1986; Cuta et al., 1995), etching is an improved method. Some advantages include batch processing, surface contouring, and a complete lack of debris formation. Furthermore, higher channel aspect ratios can be achieved with etching.

Tuckerman and Pease (1981) and Tuckerman (1984) pioneered the anisotropic etching of rectangular microchannels and the precision micromachining of micro pin fins, both in silicon, producing channels in width ranging from 50 to 102.5 μm. Their primary configuration ($w_{ch} = 50$ μm, nominally) was tested at flow rates of 4.7, 6.5, and 8.6 cm^3/s. They measured a thermal resistance of 0.090°C/W, which for a heat flux of 790 W/cm^2 maintains a temperature rise across the system ($T_h - T_{m,i}$) of 71°C. Tuckerman (1984) also showed that a microcapillary thermal interface could be used to reduce the thermal contact resistance in traditional systems for electronic cooling, where the heat source and cold plate are separate.

Wu and Little (1983) determined the friction factor for gas flow in test components with a single microchannel, either trapezoidal or nominally rectangular in cross-section. In the various test components the microchannels measured 133–200 μm wide and 28–65 μm deep. Their results for laminar flow were higher than predicted. Furthermore, they found that the transition Reynolds number is between 350 and 900 for rough channels, depending on the magnitude of the roughness. They suggested that these differences were caused by the size and nature of the channel roughness. Their results for turbulent flow were somewhat inconclusive because the channel roughness was not directly measured. Wu and Little (1984) reported the Nusselt number in counterflow heat exchangers arranged with two channels, nominally rectangular in cross-section. In various test components the microchannels were 312–572 μm wide and 89–97 μm deep. For fully developed flow in the laminar regime the Nusselt number varied rapidly with the Reynolds number, rather than obtaining a constant value. In the turbulent regime the slope was correct, however the Nusselt number was higher than predicted. They concluded that deviations from theory might be due to asymmetric wall roughness and non-uniform wall heating conditions.

Pfahler et al. (1990a, b, 1991) examined the laminar flow characteristics of several liquids in systems with a single trapezoidal microchannel, nominally 100 μm wide and 0.5–50 μm deep. In general, they found the Poiseuille number, fRe, to be lower than predicted but independent of the Reynolds number. This effect seemed to intensify as the channel depth decreased. One test section ($b = 0.8$ μm) showed a considerably higher friction factor than predicted, but the results were later attributed to channel plugging. They concluded that thermophysical property variations and entrance length considerations produced the observed effects. Their conclusions imply that the continuum assumption is valid and that the classical solutions apply to liquid flow in microchannels.

Choi et al. (1991) studied the convective heat transfer of air flow in circular microtubes, where the diameter ranged from 3 to 81 μm. In the laminar regime the Poiseuille number, fRe, was lower than predicted, while the turbulent regime results were fairly scattered. Just as Wu and Little (1984) experienced, the Nusselt number reported by Choi et al. (1991) was highly dependent on the Reynolds number in the laminar regime and was larger than predicted in the turbulent regime. Yu et al. (1995) studied the friction and heat transfer characteristics of both nitrogen and water in circular microtubes, where the diameter ranged from 19 to 102 μm. In the laminar regime their results for the Poiseuille number, fRe, were 19% lower than predicted. The friction factor in the transition and turbulent regimes was only slightly lower, about 5%. The Nusselt number, only obtained in the turbulent regime, was higher than predicted, where the deviation from theory increased as the Reynolds number increased.

Rahman and Gui (1993a, b) examined forced convection water flow in 1 mm wide trapezoidal microchannels with channel depths ranging between 79 and 325 μm in either parallel channel or single channel multipass configurations. The friction factor data as presented appear inconclusive. Heat transfer results were presented for both axially local and system averaged data. As compared to theoretical solutions, their results for the Nusselt number were high in the laminar regime and low in the turbulent regime. Their data do not show a marked increase in Nusselt number at the transition Reynolds number, which they attributed to small length scales that inhibit the growth of turbulent eddies. Gui and Scaringe (1995) performed further analysis on the data of (Rahman and Gui, 1993a, b). By reexamining the friction factor results, they determined that the critical Reynolds number was 1400. Furthermore, these results were found to agree well with theoretical solutions in the laminar regime, but became scattered in the turbulent regime. The previously reported trends for the Nusselt number were also reemphasized.

In summary, the literature is becoming increasingly rich in microchannel studies. However, as shown, the results are often conflicting, especially considering their performance as compared to classical theory in both the laminar and turbulent regimes. Our experiments involving deep microchannels show the applicability of the classical flow and convective heat transfer relations, using a dual format approach, with results presented in terms of both system and convection parameters. See Harms et al. (1997) and Harms (1997) for a review of works in which thermal performance is reported chiefly in terms of thermal resistance. The flow regime investigated in this study includes laminar and turbulent flow. Also, the effect of both the hydrodynamic and thermal boundary layer growth on the experimental results is considered. However, before the experimental results are presented the following theory is developed to provide insight into microchannel performance and for later comparison.

2. Analysis

A fairly simple one-dimensional thermal resistance model is employed to theoretically predict the frictional and heat transfer characteristics of the system of interest, shown in Figs. 1 and 2. At any axial location the system performance can be evaluated, where the friction factor and Nusselt number are obtained from appropriate developing flow solutions in the

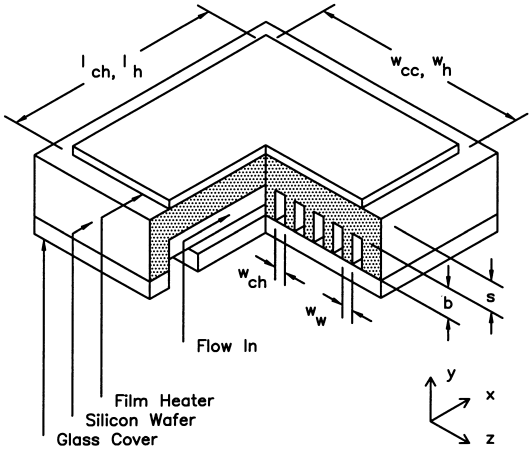

Fig. 1. A sectioned view of a rectangular microchannel heat exchanger (a multiple channel system is shown).

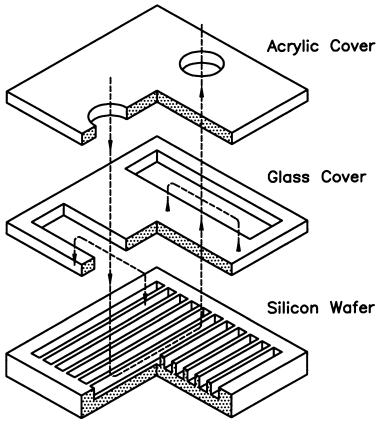

Fig. 2. An exploded view of a rectangular microchannel heat exchanger, including the manifold design (note that the orientation of the system is reversed compared to that of Fig. 1).

laminar regime and from appropriate fully developed turbulent correlations otherwise. The analysis is conjugate in the sense that convection at the water–substrate interface is simultaneously considered with conduction in the substrate.

2.1. Hydrodynamic considerations

The channel aspect ratio, α, Reynolds number, Re, and dimensionless axial distance for the hydrodynamic entrance region, x^+, are defined as

$$\alpha = w_{ch}/b \quad 0 \leqslant \alpha \leqslant 1, \tag{1}$$

$$\mathrm{Re} = U_m D_h/v, \tag{2}$$

$$x^+ = 1_{ch}/D_h\,\mathrm{Re}. \tag{3}$$

The Fanning friction factor accounts for flow restriction due to wall shear stress, τ_{wall},

$$f = 2\tau_{wall}/\rho U_m^2. \tag{4}$$

The apparent friction factor, f_{app}, is a more convenient definition (based on Δp) because it includes the momentum defect caused by the acceleration of the fluid in the entrance region. Correlations of the apparent friction factor for laminar flow in channels are obtained using solutions presented in Shah and London (1978). A correction for temperature-dependent viscosity in rectangular ducts of various aspect ratios was reported by Nakamura et al. (1979). This correction accounts for the flattened velocity profile due to lower fluid viscosity at the wall. Compared to the constant property case, this decrease in viscosity at the wall reduces the friction factor. For turbulent flow, estimation of the friction factor in rough ducts is given by Haaland (1983). For convenience, the channel surface roughness is taken as the equivalent sand grain roughness, commonly used to estimate turbulent friction in rough ducts,

$$f_{app}\,\mathrm{Re} = (\mu_w/\mu_m)^{0.58}16/G + K_\infty/4x^+, \quad x^+ \geqslant 0.1, \tag{5a}$$

$$f_{app}\,\mathrm{Re} = 11.3(x^+)^{-0.202}\alpha^{-0.094}, \quad 0.02 \leqslant x^+ < 0.1, \tag{5b}$$

$$f_{app}\,\mathrm{Re} = 5.26(x^+)^{-0.434}\alpha^{-0.010}, \quad 0.001 < x^+ < 0.02. \tag{5c}$$

$$f_{turb}^{-1/2} = 3.474 - 1.564\ln\left[(2\epsilon/GD_h)^{1.11} + 63.64/G\,\mathrm{Re}\right]. \tag{6}$$

The function G is an approximation of the exact series solution of fully developed flow in rectangular ducts (Jones, 1976). For turbulent flow, Jones showed that a modified hydraulic diameter, GD_h, better predicts the turbulent friction factor in smooth ducts, and theorizes that the same is true for rough duct correlations. The function K_∞, the incremental pressure drop number, is a correlation of results obtained from an integral analysis of developing flow (Miller and Han, 1971). This function accounts for the mentioned momentum defect,

$$G = 2/3 + (11/24)\alpha(2-\alpha), \tag{7}$$

$$K_\infty = -0.906\alpha^2 + 1.693\alpha + 0.649. \tag{8}$$

The pressure drop across the channel core is given as

$$\Delta p_{ch} = 2\rho U_m^2 f l_{ch}/D_h. \tag{9}$$

2.2. Thermal considerations

The dimensionless axial distance for the thermal entrance region is defined as

$$X^* = X/D_h\,\mathrm{Re}\,\mathrm{Pr}. \tag{10}$$

Correlations of the local Nusselt number for laminar flow in ducts are also obtained using solutions presented in Shah and London (1978). The two sets of laminar relations account for differences in the geometry and boundary conditions of the two systems. For turbulent flow, estimation of the Nusselt number in smooth ducts is given by the Gnielinski (1976) correlation, applicable to both systems of interest,

$$\mathrm{Nu}_{N=1} = 5.39, \quad X^* \geqslant 0.1, \tag{11a}$$

$$\mathrm{Nu}_{N=1} = 5.16 + 0.02(X^*)^{-1.035}, \quad 0.01 \leqslant X^* < 0.1, \tag{11b}$$

$$\mathrm{Nu}_{N=1} = 1.17(X^*)^{-0.401}\mathrm{Pr}^{-0.044}, \quad 0.001 < X^* < 0.01, \tag{11c}$$

$$\mathrm{Nu} = 8.24 - 16.8\alpha + 25.4\alpha^2 - 20.4\alpha^3 + 8.70\alpha^4, \quad X^* \geqslant 0.1, \tag{12a}$$

$$\mathrm{Nu} = 3.35(X^*)^{-0.130}\alpha^{-0.120}\mathrm{Pr}^{-0.038}, \quad 0.013 \leqslant X^* < 0.1, \tag{12b}$$

$$\mathrm{Nu} = 1.87(X^*)^{-0.300}\alpha^{-0.056}\mathrm{Pr}^{-0.036}, \quad 0.005 < X^* < 0.013. \tag{12c}$$

$$\mathrm{Nu}_{turb} = \frac{(f/2)(\mathrm{Re}-1000)\mathrm{Pr}}{1 + 12.7(f/2)^{1/2}(\mathrm{Pr}^{2/3}-1)}. \tag{13}$$

The local heat transfer coefficient is defined as

$$h = \mathrm{Nu} k_w / D_h. \quad (14)$$

The fluid temperature rise in the axial direction (Eq. (15)) is linear in systems where the boundary conditions can be approximated by a constant wall heat flux. The outlet water temperature (Eq. (16)) is given by an overall system energy balance,

$$T_m = T_{m,i} + (x/l_{ch})(T_{m,o} - T_{m,i}), \quad (15)$$

$$T_{m,o} = T_{m,i} + q/\rho Q c_p. \quad (16)$$

The region of silicon between the channels is treated as a one-dimensional fin with an adiabatic tip. Solving the fin equation gives the fin parameter and the fin efficiency. The channel resistance (Eq. (19)) follows assuming parallel thermal paths for the fin area and the exposed portion of the base area. For simplicity, the heat transfer coefficient is taken as constant along the channel cross-section. In reality, this will vary and for our configuration may result in a 4–28% difference in the fin efficiency (Huang and Shah, 1992),

$$\mathrm{mb} = (2h/k_{si} W_W)^{1/2} b, \quad (17)$$

$$\eta = \tanh(\mathrm{mb})/(\mathrm{mb}), \quad (18)$$

$$R_{ch} = [\eta h 2 b l_{ch}(N-1) + h W_{ch} l_{ch} N]^{-1}. \quad (19)$$

The substrate resistance, the local system resistance, and the heater temperature are given by

$$R_{sub} = s/k_{si} l_h W_h, \quad (20)$$

$$R = R_{ch} + R_{sub}, \quad (21)$$

$$T_h = qR + T_m. \quad (22)$$

3. Test sections

The microchannels of the present investigation were fabricated in a 2 mm thick, (1 1 0) silicon substrate by means of chemical etching, which as a consequence of crystal orientation provides rectangular channels. Two configurations were tested, a single channel system and a multiple channel system. The two types are identical except for the lack of extended surfaces in the case of the single channel system. Indeed, in both systems the channels are approximately 1000 μm deep. All channel dimensions (see Table 1) were measured using an optical microscope with micrometer stage controls.

The channels cover a total projected channel area of 2.5 cm × 2.5 cm, while the silicon substrate measures 2.9 cm × 2.9 cm, leaving only a 2 mm wide edge surrounding the channel area. A thin-film heater is deposited onto the back side of the silicon substrate, corresponding to the entire projected channel area. In much of the literature the heater area is significantly smaller than the projected channel area. This is a concern because defining the total thermal resistance as $(T_h - T_m)/q$ implicitly assumes a one-dimensional system. In systems with a small heater area compared to the projected channel area, three-dimensional conduction occurs in the substrate. Due to this thermal spreading, the maximum heater temperature and thus the thermal resistance will be lower, as compared to systems where the two areas are equal.

The channels are covered by electrostatically bonding a glass plate (containing large inlet and outlet manifolds) to the substrate, Fig. 2. The heat sink is further adhered to an acrylic block, providing convenient water connections. The heater is connected to terminal blocks by way of very fine wire bonds, and is insulated with a Teflon layer. A backing plate holds the covered channels and heater insulation securely to the acrylic block, maintaining a water tight seal.

4. Data reduction

The experimental results (at nominally constant values of input power, $q \sim 400$ W, and inlet water temperature, $T_{m,i} \sim 20$°C) for the single channel and multiple channel systems are listed in Table 2 and Table 3, respectively. The power of the main heater is determined by the product of the current, measured by the power supply, and the voltage, measured by a potentiometer. All temperatures are measured using copper/constantan (type T) thermocouples. The inlet and outlet water temperatures are measured directly at the inlet and outlet streams, respectively, while the bulk water temperature at an arbitrary axial location along the channel is calculated by Eq. (15). The heater temperature is measured using four thermocouples attached directly to the surface, two each at both $x/l_{ch} = 0.25$ and 0.75 locations. The heater temperature at a given axial location is calculated by averaging the two readings at that location. Any heat loss to the ambient would greatly affect the heater temperature, but this was found to be negligible as the measured enthalpy for all flow rates very nearly balanced the heater input (see Figs. 6 and 3 of Harms, 1997 for a plot of this comparison). Pressure is measured using either a differential pressure transducer ($\Delta p > 16$ kPa) or a manometer, depending on the range. Manometer readings are converted to pressure using the hydrostatic equation. Volumetric flow rate is measured using either a turbine flow meter ($Q > 25$ cm^3/s) or a digital scale and stopwatch, again depending on the range. For the time-averaged method, the resulting mass flow rate is divided by the density. The Reynolds number, dimensionless axial distance for the hydrodynamic entrance region, apparent friction factor, and dimensionless axial distance for the thermal entrance region are given by Eqs. (2), (3), (9) and (10), respectively. To calculate the channel core pressure drop the manifold pressure drop must first be subtracted from the measured value. The inlet and outlet manifold pressure drop includes expansion, contraction, and bend losses in the transition regions between the circular inlet and outlet and the channel core (see Harms, 1997 for more details), which are mainly determined from empirical relations (Blevins, 1984).

The local system resistance can be determined from Eq. (22) (knowing T_h, T_m, and q). One should be aware that the definition of thermal resistance is not unique among

Table 1
Dimensions of the two tested microchannel configurations

N	b (μm)	w_{ch} (μm)	w_w (μm)	α	A (cm^2)	D_h (μm)	ϵ/D_h
1	1000	25 000	–	0.040[a]	6.25	1923	~0
68	1030	251	119	0.244	39.30	404	0.020

[a] $\alpha = b/w_{ch}$ to satisfy the fractional constraint in Eq. (1).

Table 2
Experimental flow and heat transfer results for the single channel system (italics denote transitional flow regime)

Exp. no.	Q (cm^3/s)	$T_{m,o}-T_{m,i}$ (°C)	Re_D	Δp (kPa)	f	R (°C/W)	Nu
1	16.1	1.9	1383	0.925	–	0.135	40.9
2	*20.1*	*2.0*	*1700*	*1.40*	–	*0.126*	*44.0*
3	25.4	1.9	2152	2.02	–	0.111	50.5
4	32.9	1.5	2760	3.35	–	0.097	58.8
5	43.1	1.1	3619	5.62	–	0.083	69.8
6	56.2	0.9	4691	9.36	–	0.072	82.8
7	72.4	0.7	5995	14.5	–	0.062	98.2
8	93.7	0.6	7751	22.5	–	0.055	115
9	120	0.5	9937	35.6	–	0.048	138
10	156	0.4	12 900	61.2	–	0.043	159

Table 3
Experimental flow and heat transfer results for the multiple channel system (italics denote transitional flow regime)

Exp. no.	Q (cm^3/s)	$T_{m,o}-T_{m,i}$ (°C)	Re_D	Δp (kPa)	f	R (°C/W)	Nu
1	5.47	13.3	173	1.22	0.0812	0.097	2.65
2	7.46	11.4	228	1.85	0.0604	0.087	3.01
3	9.57	8.9	279	2.66	0.0503	0.080	3.35
4	12.0	8.1	344	3.74	0.0431	0.069	4.01
5	14.7	6.5	411	5.12	0.0367	0.063	4.44
6	18.0	5.4	491	6.92	0.0311	0.058	4.92
7	21.9	4.4	588	9.60	0.0286	0.053	5.63
8	28.8	3.3	755	14.0	0.0219	0.048	6.64
9	36.8	2.5	953	20.9	0.0192	0.044	7.46
10	46.3	1.9	1188	30.5	0.0170	0.041	8.41
11	*59.0*	*1.5*	*1510*	*48.0*	*0.0167*	*0.038*	*9.57*
12	75.7	1.0	1947	76.7	0.0165	0.035	11.6
13	93.4	0.7	2438	112	0.0157	0.034	14.2
14	118	0.5	3169	169	0.0147	0.032	17.6

investigators. Many researchers define the characteristic temperature difference as the difference between the inlet water temperature and the maximum heater temperature. A more representative definition of this difference for our one-dimensional thermal resistance network is $T_h(x) - T_m(x)$. The previous definition is overly conservative in that it includes a so called thermal resistance due to the increase in the water temperature along the axial direction. This rise is strictly a consequence of the conservation of energy and as such should be treated separately. However, for the sake of completeness, be aware that the total thermal resistance (based on $T_{m,i}$) has been reported in Harms (1997) for each experiment, along with a discussion and critical comparison of the local and total values of thermal resistance.

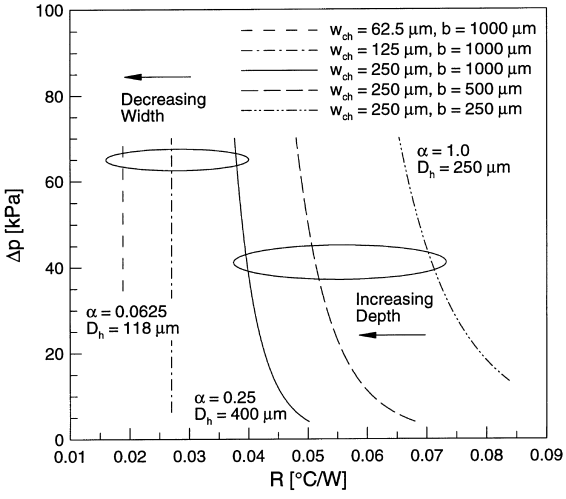

Fig. 3. A parametric analysis based on the theoretical model showing the effect of channel width and channel depth: pressure drop as a function of thermal resistance.

Experimentally, the local heat transfer coefficient is determined from Newton's law of cooling,

$$h = q/A(T_W - T_m). \tag{23}$$

In this situation the area available for convection, A, and the temperature at the silicon–water interface, T_w, depend on the type of channel configuration and are defined as,

$$A = l_{ch}W_{ch}, \quad \text{single channel,} \tag{24a}$$

$$A = Nl_{ch}(W_{ch} + 2b), \quad \text{multiple channels,} \tag{24b}$$

$$T_w = T_h - qR_{sub}, \quad \text{single channel,} \tag{25a}$$

$$T_w = T_m + \eta(T_h - qR_{sub} - T_m), \quad \text{multiple channels.} \tag{25b}$$

In the single channel design T_w is determined by subtracting the temperature drop across the substrate from the measured heater temperature. In the multiple channel system the average wall temperature is determined by integrating the solution to the fin equation. Doing so will reveal a second interpretation of fin efficiency which directly relates to the average wall temperature. One should note that this reduction only holds for one-dimensional systems. With the above reductions the Nusselt number can be determined from Eq. (14).

An uncertainty analysis was performed on all the relevant parameters in accordance with the procedure described by Moffat (1988). Although each data point has an associated uncertainty, only the maximum values of uncertainty are presented here. The bias limits (fixed error) of the pressure measurements dominated the total uncertainty of both the manometer, 2.7%, and the differential pressure transducer, 5.3%. Alternately, the precision limits (random error) of the volumetric flow rate measurements dominated the total uncertainty of both the time-average method, 3.3%, and the turbine flow meter, 2.6%. The Reynolds number uncertainty, 3.4%, follows from the volumetric flow rate uncertainties. Discounting the effect of the manifolds, the friction factor uncertainty is 8.5%. As expected, the bias limit of the temperature measurements, ±0.5°C, contributes significantly to the Nusselt number uncertainty, 5.5%. Note that the uncertainty associated with Eq. (25) is not included in this analysis.

5. Results and discussion

To determine preferred geometric configurations, the theoretical model is first evaluated in a parametric fashion to generate the dependent variables of pressure drop and thermal resistance over a large range of flow rates. In Fig. 3 the pressure drop results are plotted as a function of thermal resistance for three different channel widths and three different channel depths. Each curve was generated by varying the flow rate at 1 cm^3/s intervals starting at 5 cm^3/s. For the two smaller channel configurations ($w_{ch} = 62.5$ and 125 μm) fully developed conditions prevail for the vast majority of the channel over the analyzed flow range. Therefore, the thermal resistance is independent of the flow parameters. In these cases the performance limitation is set by the water temperature difference, which is only a function of input power and flow rate. For this reason the individual data sets are restricted to $Q \geqslant 5$ cm^3/s. With this limitation the 125 mm wide channel configuration provides the best combination of low pressure drop and low thermal resistance. In contrast to the smaller widths, the temperature profile of the large channel (solid line, $w_{ch} = 250$ μm) is developing over the entire flow range of interest. As a result the pressure drop and the thermal resistance are inversely related. Overall, the thermal resistance decreases as the channel width decreases for a fixed channel depth, which is expected as the heat transfer coefficient is directly proportional to the hydraulic diameter. Moreover, the area available for convection increases as the channel width decreases due to an increase in the number of channels. Changes in aspect ratio also support the mentioned trend by increasing the Nusselt number (Nu increases as α decreases), but this effect is of secondary importance.

The pressure drop as a function of thermal resistance is also plotted in Fig. 3 for three different channel depths. Again, a strong inverse relationship between pressure drop and thermal resistance is evident for wide channel configurations due to developing flow conditions. Overall, for a constant value of pressure drop, the thermal resistance decreases substantially as the channel depth increases. This trend is mainly due to increases in the area available for convection. Interestingly, changes in aspect ratio support the trend while changes in hydraulic diameter resist the trend, but both of these changes are of second order in effect. Clearly this comparison shows that deeper channels provide better flow and heat transfer performance. However, one should remember that several approximations were made in developing the theoretical model. Thus, caution should be used in applying these results.

Experimentally, both a single channel design (Table 2) and a multiple channel design (Table 3) were tested for this study. In these tables the results are delineated to emphasize the laminar, transitional, and turbulent flow regimes. The results in Table 2 of the single channel design mostly fall in the turbulent regime. In contrast, developing laminar flow prevails in the majority of the data for the multiple channel design in Table 3. Both sets of results demonstrate the inverse relationship between flow rate and water temperature difference. At low flow rates ($Q < 12$ cm^3/s, Table 3) the system temperatures exhibit significant non-uniformity in the axial direction. In this sense, higher flow rates are preferred. Of the preferred operating conditions in Table 3, Exp. nos. 4–10, the water temperature rise is seen to be much lower, from 1.9°C to 8.1°C. Use of this configuration in the turbulent regime is not recommended due to only marginal reductions in R for significant increases in Δp. For example, comparing Exp. nos. 10 and 12, R decreases by 15% while Δp increases by 250%. Increasing Q further, comparing Exp. nos. 12 and 13, results in even less return; R decreases by 3% while Δp increases by 150%.

The friction factor of the multiple channel design is reported in Fig. 4 as a function of the Reynolds number. Note that the friction factor of the single channel design could not be determined due to the relatively large manifold pressure drop as compared to Δp_{ch}. Regarding the multiple channel friction factor, the most striking result is the clear transition from laminar flow to transitional flow at a Reynolds number of about 1500. This is lower than the value of 2400 reported by Allen and Grunberg (1937) for rectangular ducts ($\alpha = 0.256$) with an abrupt entrance; nonetheless, the severity of the inlet condition is known to have a significant effect on the critical Reynolds number. Furthermore, other investigators have found similar results for microchannels. Wu and Little (1983) found that transition occurred between a critical Reynolds number of 350 and 900, depending on the channel roughness (the actual roughness values were not measured). Gui and Scaringe (1995) determined the critical Reynolds number to be 1400, which they also attributed to channel roughness. Again, ϵ was not measured explicitly, but they suggested that $\epsilon/D_h \approx 0.015$. Even though the relative roughness of the multiple channel system is appreciable ($\epsilon/D_h = 0.020$, determined via profilometer measurements), the stated difference in critical Reynolds number is attributed to a severe inlet condition.

One important consideration in isolating the friction factor is the estimation of the manifold pressure drop. At low flow

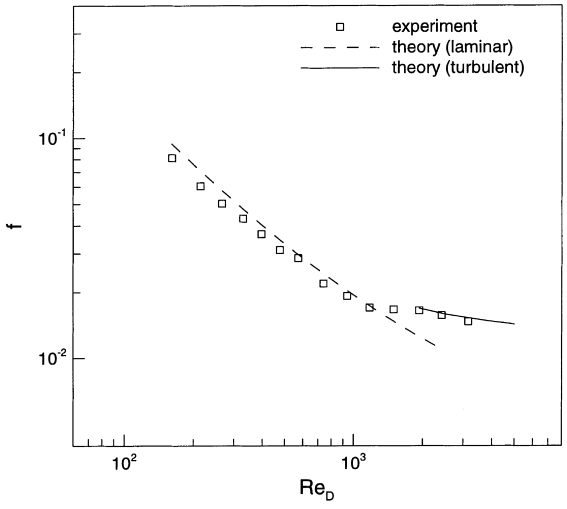

Fig. 4. The friction factor as a function of the Reynolds number for the multiple channel system.

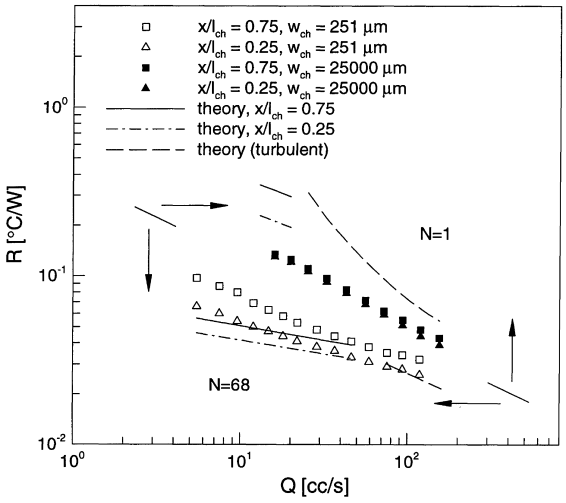

Fig. 5. Thermal resistance as a function of volumetric flow rate for both configurations.

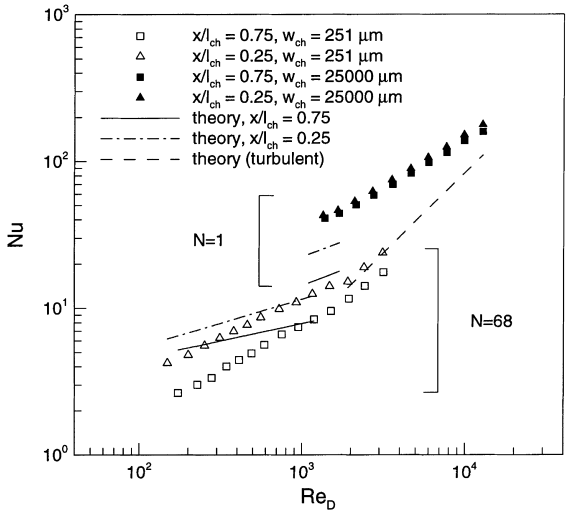

Fig. 6. The Nusselt number as a function of the Reynolds number for both configurations.

rates the channel core dominates the flow friction. In fact, in this case theory suggests that the maximum value of $\Delta p_{ch}/\Delta p$ is 93%. As such, the experimental results closely follow laminar theory. At high flow rates the manifold pressure drop is appreciable; the minimum value of $\Delta p_{ch}/\Delta p$ is 50%. If the determination of the manifold pressure drop is inaccurate, then the uncertainty of friction factor will be higher. Nonetheless, the high Reynolds number results in Fig. 4 are in excellent agreement with turbulent theory.

The local thermal resistance as a function of flow rate is presented in Fig. 5 for both configurations. For the single channel design the experimental results are significantly lower than predicted by theory for both flow regimes. This difference is most likely caused by flow impingement at the 90° inlet bend, which in turn significantly increases the convective heat transfer rate (Zhuang et al., 1997). For the multiple channel design the experimental results agree well with theory at high flow rates; however, this agreement deteriorates as the flow rate decreases. The discord with theory at low flow rates perhaps is caused by flow bypass in the manifold. At low flow rates flow bypass may exist because theory suggests that the pressure drop in the manifold is much lower than that of the core. This would result in a shorter channel flow length, which in turn would significantly increase the theoretical values of thermal resistance. In this sense, the theory breaks down but the experimental values are valid seeing that they adhere to a specific definition regardless of the validity of the one-dimensional assumption. Note that this will have less effect on the friction factor since flow bypass in the manifold still contributes to the total pressure drop. Nonetheless, the friction factor will be partially reduced by flow bypass. A closer inspection of Fig. 4 reveals that the data are consistent with this explanation, being somewhat lower than theory at low flow rates.

The local Nusselt number as a function of the Reynolds number is presented in Fig. 6 for both systems. As expected, the experimental Nusselt number for the single channel design is significantly larger than predicted. Again, this may be explained by flow structures induced by the inlet bend enhancing heat transfer. In fact, the experimental results of Zhuang et al. (1997) for parallel plate microchannels showed similar increases in the Nusselt number. Although their system also has a 90° inlet bend, a quantitative comparison is not possible as their channel dimensions are somewhat different from that of the present study. For the multiple channel design the previously discussed hypothesis, regarding the effects of flow bypass at low flow rates, also applies to the Nusselt number data. However, since the Nusselt number is inversely related to thermal resistance, the experimental results are lower than, instead of higher than, the theoretical values. In contrast to the results in terms of thermal resistance (Eq. (5)), we believe that the convective heat transfer theory (Fig. 6) is applicable. Furthermore, since the inlet manifold region does not provide adequate flow conditioning, the experimental values are in error. In the turbulent regime, where the inlet condition has less impact, the agreement between theory and experiment is much better. As expected, the results for both axial locations tend to collapse to a single curve. As with the friction factor, but to a lesser degree, one can observe a transition at a critical Reynolds number of 1500.

The local Nusselt number for the multiple channel design is considered further in Fig. 7, now plotted with respect to the dimensionless axial distance. Only the laminar regime data are shown as the fully developed turbulent results are not appropriate in a developing heat transfer analysis. The thermal

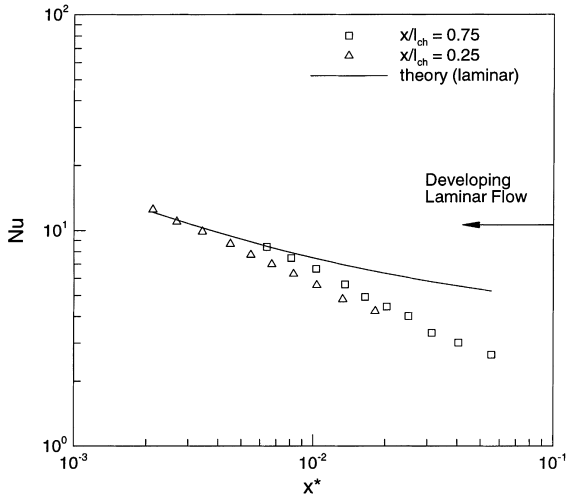

Fig. 7. The Nusselt number as a function of dimensionless axial distance for the multiple channel system.

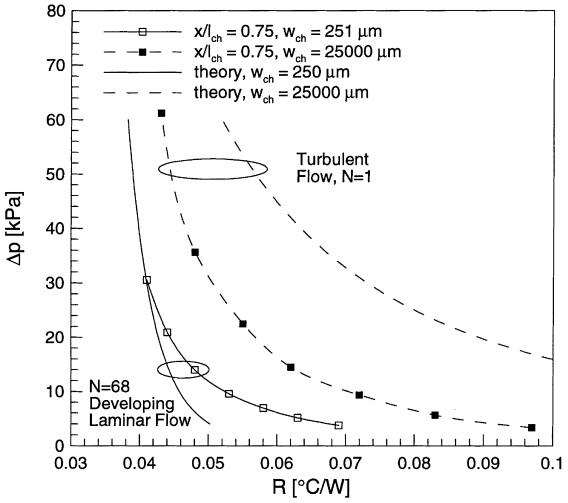

Fig. 8. Selected experimental and analytical results for both systems: pressure drop as a function of thermal resistance.

entrance region should not be a factor in the turbulent regime because the turbulent thermal boundary layer develops very quickly. Cebeci and Bradshaw (1988) suggest that fully developed turbulent conditions prevail when $x/D_h = 5$ (in our system $l_{ch}/D_h = 62$). In contrast, the effect of the thermal entrance region in the laminar regime is significant ($x^* < 0.1$ across the entire range). Note that the relationship between theory and experiment is consistent with Fig. 6 because x^* increases as flow rate decreases. As expected, the results for both axial locations tend to collapse to a single curve.

Both systems are directly compared against each other (and theory) in Fig. 8 over their preferred operating range, Exp. nos. 4–10 for both arrangements. As illustrated in Fig. 3, plotting pressure drop against thermal resistance is the best way to compare systems because these are the competing factors in any practical design. Although the trend in both data sets appears very similar, the behavior seen for the multiple channel system is a result of developing laminar flow, while the observed trend of the single channel system is a result of turbulent flow and its inherent dependence on the Reynolds number. Certainly, the comparison illustrated by this figure shows that developing laminar flow designs utilizing deep microchannels perform better than turbulent single channel flow designs, over the given range of flow rates. This is attributed to the decreased hydraulic diameter and the increased surface area of the multiple channel system, despite the much higher Nusselt number of the turbulent single channel system.

6. Conclusions

The hydrodynamic and thermal performance of two deep microchannel configurations have been reported, both theoretically and experimentally. A parametric analysis based on the theoretical model was used to identify preferred configurations of the multiple channel design. For fully developed laminar flow the thermal resistance is independent of the pressure drop. As such the performance limit is set by the allowable temperature difference across the ends of the system. In contrast, an inverse relationship between pressure drop and thermal resistance is noted for the developing laminar flow results. Moreover, the analysis showed that decreasing the channel width and increasing the channel depth provide better flow and heat transfer performance.

For the multiple channel design the experimental friction factor follows the theoretical values reasonably well in both the laminar and turbulent regimes. Furthermore, a clear transition is evident in the plot of the experimental friction factor at a critical Reynolds number of 1500, which is lower than the value of 2400 reported for conventional channels. In this case the critical Reynolds number is believed to have been altered by the severity of the inlet condition. The effect of the manifold on the character of the flow is also suggested to be the reason for the somewhat lower than predicted values of friction factor at low flow rates. Both of these results reflect the importance of manifold design in microchannel systems.

For both designs the experimental Nusselt number agreement with theory was a bit lacking, but on the other hand, cannot be discarded. For the single channel design the experimental Nusselt number was higher than predicted at all flow rates. This enhancement may be due to the effect of the inlet bend. The results for the multiple channel design agree reasonably well with theory at high flow rates, but deviate significantly from theory at low flow rates. This deviation was attributed to flow bypass in the manifold. Nonetheless, we still feel that the classical relations for local Nusselt number are appropriate and accurate for modeling microchannel systems, given the right manifold design.

Finally, the two systems were critically compared. The experiments showed that in both designs, pressure drop is inversely related to thermal resistance. As such, increasing the pressure drop beyond the region of rapid curvature at the high flow rate end of the trend results in diminishing returns. Conversely, at very low flow rates the thermal resistance can be significantly lowered by slightly increasing the allowable pressure drop. Notably, the thermal resistance of the multiple channel design is always lower than that of the single channel design, for a given level of pressure drop. This indicates that for our systems developing laminar flow provides better overall performance than turbulent flow.

Acknowledgements

The support of this research by NASA through grant #NAG3-1706 is appreciated. The authors also wish to acknowledge the expert fabrication of both test components by Alexander Hölke, Ph.D. candidate in Electrical Engineering at the University of Cincinnati.

References

Allen, J., Grunberg, N.D., 1937. The resistance to the flow of water along smooth rectangular passages and the effect of a slight convergence or divergence of the boundaries. Philos. Mag. 23, 490–502.

Blevins, R.D., 1984. Applied Fluid Dynamics Handbook. Van Nostrand Reinhold, New York.

Cebeci, T., Bradshaw, P., 1988. Physical and Computational Aspects of Convective Heat Transfer. Springer, New York.

Choi, S.B., Barron, R.F., Warrington, R.O., 1991. Fluid flow and heat transfer in microtubes. ASME DSC 32, 123–134.

Cuta, J.M., Bennett, W.D., McDonald, C.E., Ravigururajan, T.S., 1995. Fabrication and testing of micro-channel heat exchangers. SPIE 2640, 152–160.

Gnielinski, V., 1976. New equations for heat and mass transfer in turbulent pipe and channel flow. Int. Chem. Eng. 16, 359–368.

Gui, F., Scaringe, R.P., 1995. Enhanced heat transfer in the entrance region of microchannels. Proceedings of the 30th Intersociety Energy Conversion Eng. Conf. 2, 289–294.

Haaland, S.E., 1983. Simple and explicit formulas for the friction factor in turbulent pipe flow. J. Fluids Eng. 105, 89–90.

Harms, T.M., 1997. Heat transfer and fluid flow in deep rectangular liquid-cooled microchannels etched in a (110) silicon substrate. M.S. thesis, University of Cincinnati, Cincinnati.

Harms, T.M., Kazmierczak, M., Gerner, F.M., Hölke, A., Henderson, H.T., Pilchowski, J., Baker, K., 1997. Experimental investigation of heat transfer and pressure drop through deep rectangular microchannels in a (110) silicon substrate. ASME HTD 351, 347–357.

Hölke, A.D., 1998. Development of silicon chemical wet etching technology towards the realization of an integrated thermal-electronic packaging system. Ph.D. thesis, University of Cincinnati, Cincinnati.

Huang, L.J., Shah, R.K., 1992. Assessment of calculation methods for efficiency of straight fins of rectangular profile. Int. J. Heat and Fluid Flow 13, 282–293.

Jones, O.C., 1976. An improvement in the calculation of turbulent friction in rectangular ducts. J. Fluids Eng. 98, 173–181.

Miller, R.W., Han, L.S., 1971. Pressure losses for laminar flow in the entrance region of ducts of rectangular and equilateral triangular cross section. J. Appl. Mech. 38, 1083–1087.

Moffat, R.J., 1988. Describing the uncertainties in experimental results. Exp. Thermal Fluid Sci. 1, 3–17.

Nakamura, H., Matsuura, A., Kiwaki, J., Matsuda, N., Hiraoka, S., Yamada, I., 1979. The effect of variable viscosity on laminar flow and heat transfer in rectangular ducts. J. Chem. Eng. Japan 12, 14–18.

Pfahler, J., Harley, J., Bau, H., Zemel, J., 1990a. Liquid transport in micron and submicron channels. Sensors and Actuators A 22, 431–434.

Pfahler, J., Harley, J., Bau, H.H., Zemel, J., 1990b. Liquid and gas transport in small channels. ASME DSC 19, 149–157.

Pfahler, J., Harley, J., Bau, H., Zemel, J.N., 1991. Gas and liquid flow in small channels. ASME DSC 32, 49–60.

Rahman, M.M., Gui, F., 1993a. Experimental measurements of fluid flow and heat transfer in microchannel cooling passages in a chip substrate. ASME EEP 4 (2), 685–692.

Rahman., M.M., Gui, F., 1993b. Design, fabrication, and testing of microchannel heat sinks for aircraft avionics cooling. Proceedings of the 28th Intersociety Energy Conversion Eng. Conf. 1, 1–6.

Sasaki, S., Kishimoto, T., 1986. Optimal structure for microgrooved cooling fin for high-power LSI devices. Electron. Lett. 22, 1332–1334.

Shah, R.K., London, A.L., 1978. Advances in Heat Transfer, Supplement 1: Laminar Flow Forced Convection in Ducts. Academic Press, New York.

Tuckerman, D.B., 1984. Heat-transfer microstructures for integrated circuits. Ph.D. thesis, Stanford University, Stanford.

Tuckerman, D.B., Pease, R.F.W., 1981. High-performance heat sinking for VLSI. IEEE Electron Device Lett. 2, 126–129.

Wu, P., Little, W.A., 1983. Measurement of friction factors for the flow of gases in very fine channels used for microminiature Joule-Thomson refrigerators. Cryogenics 23, 273–277.

Wu, P., Little, W.A., 1984. Measurement of the heat transfer characteristics of gas flow in fine channel heat exchangers used for microminiature refrigerators. Cryogenics 24, 415–420.

Yu, D., Warrington, R., Barron, R., Ameel, T., 1995. An experimental and theoretical investigation of fluid flow and heat transfer in microtubes. Proceedings of the ASME/JSME Thermal Eng. Joint Conf. 1, 523–530.

Zhuang, Y., Ma, C.F., Qin, M., 1997. Experimental study on local heat transfer with liquid impingement flow in two-dimensional micro-channels. Int. J. Heat Mass Transfer 40, 4055–4059.